Research Plan

Compression after impact test in composites using acoustic emission

by

Group D5

J. Cunha	5216087
J. del Canho	5100380
L. Distelbrink	5274400
M. Fetecau	5236789
J. Korycki	5218306
B. Lee	5225604
D. Stiller	5253969
T. Teixeira Pijpers	5025249
R. van Dijk	5208130
T. van Kuik	5275547

University: TU Delft, Faculty of Aerospace Engineering
Course: AE2223-I Test, Analysis & Simulation
Due date: March 4, 2022

TU Delft

Acronyms

AE Acoustic Emission

BVID Barely Visible Impact Damage

CAI Compression After Impact

CFRP Carbon-Fiber-Reinforced Polymer

FFT Fast Fourier Transform

LDA Linear Discriminant Analysis

NDE Non-Destructive Evaluation

PCA Principle Component Analysis

RPCA Robust Principle Component Analysis

1. Introduction

The aircraft industry has seen a rapid growth in the adoption of composite materials such as CFRP [1]. The main feature of composites that attracts designers is their excellent strength at lower weights, lower than even aluminium alloys, leading to higher fuel efficiency. This trend has led to aircrafts like the Airbus A350, in which composites account for around 53% of its airframe mass [2]. The study of impacts on composite structures is therefore a topic of great and growing interest in the field of aviation.

During the production, operation and maintenance of aircraft, various types of impacts occur on its composite parts. Small and medium velocity impacts occur fairly often due to runway debris or dropped tools while heavy impacts are less common. The most dangerous damage is Barely Visible Impact Damage (BVID), which can cause damage growth under fatigue and significant strength degradation, especially in compression [3]. With this aspect in mind, it is important to posses an array of Non Destructive Evaluation (NDE) techniques to monitor the onset and propagation of damage modes, alongside in-depth knowledge of damage development under loading, so that the state of damage within the structure can be accurately estimated, without dismantling the structure. Using this knowledge, it could be possible to implement a slow growth principle in the design process of composites, in order to create thinner and lighter functional parts.

Acoustic Emission (AE) has been proposed as a way to detect and differentiate the damage modes that occur during and after impact. By detecting the dynamic stress field given by an internal displacement caused by a damage mode using piezoelectric sensors, the elastic vibrations of the material can be converted to electric signals. These signals can then be filtered, amplified and have specific features extracted from them. It is believed that by using different data analysis methods, it is possible to then cluster the data points by similarity and associate them to a specific damage mode.

In this research plan, a multi-stage pipeline, accompanied by a clear methodology, are proposed as a means to accurately identify and differentiate damage modes that occur in compression testing after impact, in either static or cyclic loading. This methodology will be applied to data obtained from Compression After Impact (CAI) testing of multi-oriented ply CFRP. The validity of the method will then be tested against a labeled data set. The main goal of this investigation is to develop a well-rounded, efficient and accurate analysis method that is able to indicate the magnitude of damage mode propagation, as well as to classify each damage mode based on the features on their signal.

The research plan starts with a brief literature review Section 2 that presents some important background information on the involved topics, as well as the findings and conclusions of other authors in the past. After this theoretical review, the research questions, aim and objective of this investigation are stated in Section 3. Then, the investigated methodology of data analysis is presented and elaborated as a step by step procedure in the form of a pipeline. Section 5 describes the testing procedures that were followed in order to obtain the data that is going to be used to assess the previously stated methodology, and it is followed by Section 6 which delves into the validation procedure of the methodology, together with the determination of performance metrics to be used. The final section, Section 7, will showcase the initial planning that was conceived to be sure that the goals of the research are met.

2. State of the art/Literature review

2.1. Impact on composites

The responses in a clamped composite plate impact test have been illustrated well by Olsson [4, p. 880], where two impacts with equal energy are compared. A high-velocity low-mass impact produced a heavily oscillating response with a peak load higher than the low-velocity test. It was also shown that low-velocity large-mass impact produces a response that is virtually the same as a static test - a roughly bell-shaped load and deflection graph is created when the laminate is not penetrated [5]. This is preferred when testing the residual strength of a composite after impact.

Impact on a flat plate will result in the propagation of elastic waves from the point of contact. ”It can be shown that the response type under elastic conditions is solely dependent on the impactor/plate mass ratios” [6, p. 550]. Davies [6] explains that impactors with masses $M > M_{plate}$, categorized as large-mass, will induce a quasi-static response with in-phase deflection and load.

In addition to mass, the velocity of the impactor will also greatly alter the material response to impact. All velocities with $V < 70\,\mathrm{m}\cdot\mathrm{s}^{-1}$ are classified as ”low-velocity impacts” [6, p. 555]. These low-velocity impacts are the most serious for carbon composites which have low elastic properties and often result in BVID [6, p. 541].

Damage modes

There exists a substantial body of knowledge describing the different damage modes that can occur in composite materials, including numerous review papers [7–10]. Greenhalgh and Hiley [11] classify the damage modes in composites into translaminar, intralaminar and interlaminar. The translaminar class includes fiber fracture and kinking, while the intralaminar class includes matrix damage modes such as matrix cracking and matrix/fiber debonding. Interlaminar damage occurs between two layers in the lay-up (delamination), making it a dangerous form of BVID [6, 12]. Following an impact, all three of these classes of damage modes are likely to occur [12, p. 232].

Regarding impact testing, all the primary sources have little to no conflicting views. The procedures and categorizations of different impactors and test methods as described by Davies [6] and Olsson [4] are fairly standard through all literature.

Delamination is widely considered to be one of the more important damage modes. Liu ([13]) explained that delamination only occurs between plies with different fiber orientations. This is caused by the bending stiffness mismatch between these layers. He also found that the delaminations are mostly oblong-shaped. The same results were found in different studies as well [14–16]. When the delamination is initiated, delamination growth occurs when the impact load passes a certain threshold. After the first delamination has been initiated at the most critical interface further delaminations will occur in almost all interfaces. The large membrane strains lead to local fiber fractures near the location of impact according to Olsson [5].

When a composite undergoes low-velocity transverse impact the first type of failure which is induced is matrix damage according to Richardson and Wisheart [17, p. 1124]. This makes it another one of the most important damage modes. Matrix cracks occur due to the different properties of the matrix and the fiber. The first type of matrix cracks are caused by the high transverse shear stress which is present through the material and are inclined at a 45°angle with respect to the fiber direction. The other main type of matrix crack is caused by high tensile bending stresses and propagates perpendicular to the fiber direction [17].

Residual strength

Post-impact, the compressive strength of composite panels is reduced more than the tensile strength, especially in fatigue [12, 18, 19] This difference is due to delamination growth, which is caused by local buckling, and leads to premature buckling of the entire panel. The compressive strength after impact may be affected by as much as 70% [3, 6].

2.2. Compression after Impact

As mentioned in the previous section, the compressive strength of composites reduces significantly after impact. This happens both under static loading and fatigue. As applying a slow-growth principle to design with composites would allow for higher limit design stress, and therefore a lighter structure, it is beneficial to know how the damage grows over time and how severely the load bearing capability is compromised immediately after impact. To study this, many research groups have run compression after impact tests, in which they try to classify different damage modes using a variety of detection methods. However, because many damage types are hard to detect with common measuring equipment, often simplified relations were

set up between easily detectable damage types such as delaminations, and residual strength.

Static loading

Many static loading experiments have been performed, which have tried to classify which damage types will lead to complete failure, and will therefore be the limiting factor. One such study was conducted by Bull et al. [20]. In their test they found that the CAI performance for quasi-static loading, was largely linked to the projected delamination area after impact, and delamination growth, resulting in sub-laminar buckling. However, as Pascoe points out in his paper [21], other experiments such as those performed by Nettles and Scharber [22], indicated that the critical failure mode was fiber kinking, which initiated at the edges of delaminations due to stress concentrations. Contrary to Bull, they found no indication that delamination growth was a factor contributing to failure.

Both of these experiments used the same fibers, but different resins, which could be contributing to their differing conclusions. This also shows that the results of these experiments can not easily be generalized, as they use a specific testing setup and environment, variations in which could lead to changes in results. This is not only true between different experiments, but also between experiments and the real situation they represent, for example a CFRP airplane fuselage. For this reason, it could be dangerous to follow generalized and simplified failure load relationships, such as predicting the residual strength based purely on the projected delamination area, as Bull et al. did [20], or on the indentation depth after impact [23].

Damage propagation under cyclic loading

The influence of fatigue loading on composites is the cause of many contradictions and conflicting information. Tests performed by Isa et al. [24] and Ogasawara et al. [25] concluded that fatigue testing at low loads would result in intermittent growth, in which delaminations grow quickly at the start, plateau during most of its fatigue life and then grow accelerated near failure. Additionally, tests performed by Chen et al. [26] and Mitrovic et al. [27] showed that delamination growth was continuous during for higher loads. This observation of no-growth at lower loads and slow-growth at higher loads, was also found by Tuo et al. [28] and can be seen in Figure 1.

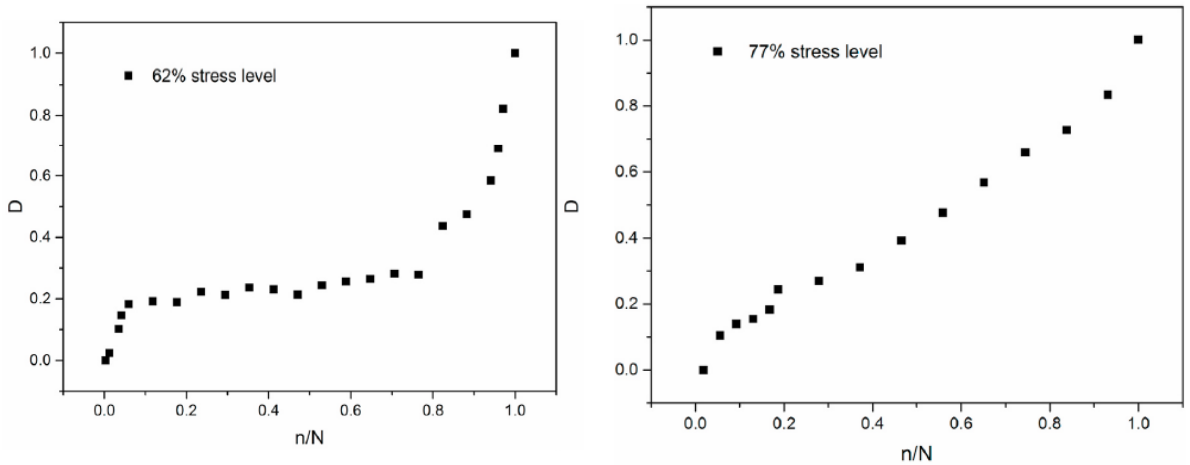

(a) *Damage evolution based on stiffness degradation under 62% stress level*

(b) *Damage evolution based on stiffness degradation under 77% stress level*

Figure 1: *Damage evolution based on stiffness degradation under two cyclic stress levels [28, p. 10].*

However, this behaviour was not seen for all laminates. Bogenfeld and Gorsky [23] showed that no-growth can also present for higher loads. In Bogenfeld and Gorsky their experiments, the damage growth for lower loads behaved similar, but the delamination growth for higher loads did not follow the slow-growth principle, as can be seen in Figure 2.

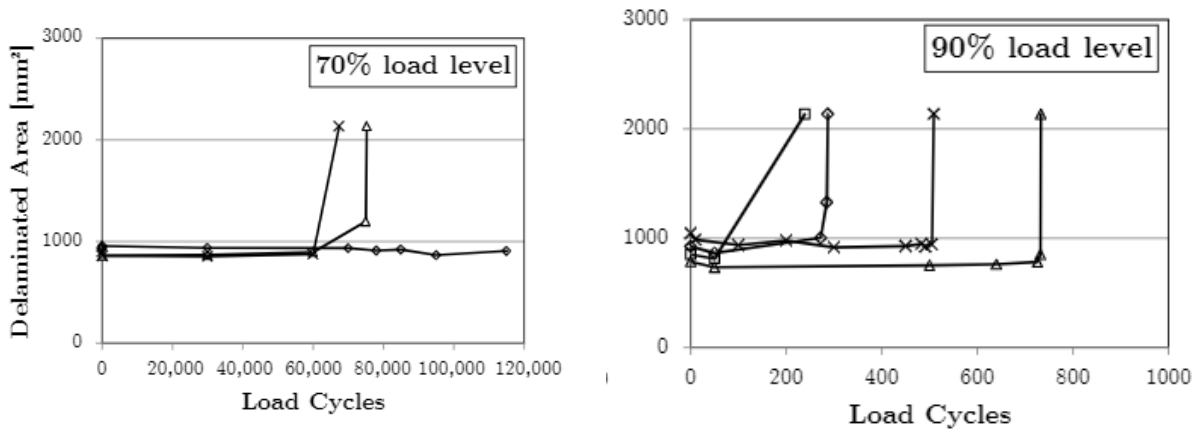

(a) *Delamination area propagation under a cyclic loading of 70%*

(b) *Delamination area propagation under a cyclic loading of 90%*

Figure 2: *Damage evolution of delamination area under two cyclic stress levels [23, p. 11].*

Despite the test having different coupons, it still shows the variance of observations and emphasizes the need for better physical understanding, rather than simplified relations predicting failure behaviour [21]. Moreover, it should be noted that delamination growth is not the whole story when it comes to damage growth in fatigue, as the materials also suffer from fatigue when no growth is observed, indicating that there is another damage mechanism at work. Thus a closer look should be taken at the complete spectrum of damage types, instead of just delaminations.

Limitations of current testing methods

As discussed in the sections above, the exact formation mechanisms and interactions between damage types in compression after impact, are still fairly unknown. Many studies such as those done by Bull et al. [20], Isa et al. [24] and Ogasawara et al. [25] try to track only a few damage types and attribute final failure to one of them, but few consider all of them. One major reason for this is that current identification methods are very limited in their capabilities. Some widely used techniques include ultrasonic c-scans, micro-graphic observation, and x-ray computed tomography [21]. Ultrasonic c-scans are widely used, but can only show delaminations, as other damage types are too small to be detected. Micro-graphic observation on the other hand allows for the identification of all damage types, but is destructive, and can only show damage in a small 2D slice of the cross-section. X-ray computed tomography can construct very detailed images of present damage, but only in a small scan volume, and requires equipment that is not widely available.

2.3. Acoustic Emissions

Acoustic Emissions represent a novel Non Destructive Evaluation technique, first mentioned in 1970 by Hagemaier et al. [29] in a study using ultrasound to detect material anomalies in graphite composites. This method is believed to be able to assess different types of damage occurring within a material, not only after impact or testing, but also during the process. Saeedifar et al. [30] defines AE as ”the propagation of a transient elastic wave within the material caused by a sudden release of strain energy which can be due to the occurrence of damage”. Thus, the elastic wave that propagates through the material can be grouped according to their similarity and interpreted so that they can be associated with a specific failure mode.

Acoustic emission recording

The process of recording these AE is eloquently presented by Eitzen and Wadley [31]. Firstly, an event, characterized by a specific failure mode caused by loading the specimen, occurs within the material. Immediately after this event, a dynamic stress field is created around the location of the event. This dynamic stress field is then propagated through the material until it reaches strategically placed broadband highly

sensible piezoelectric sensors, which emit an output voltage.

Before the acquisition of data, some steps are required to ensure the quality of the signal. Rescalvo et al. [32] gives a brief description of this pre-acquisition process. As the intensity of the AE signal is fairly low, some sort of pre-amplifying is needed to minimize signal loss and interference. Then, a certain bandwidth is selected for acquisition, filtering undesirable noise. Lastly, the signal can be amplified once more for readability purposes. These steps are visually presented in Figure 3

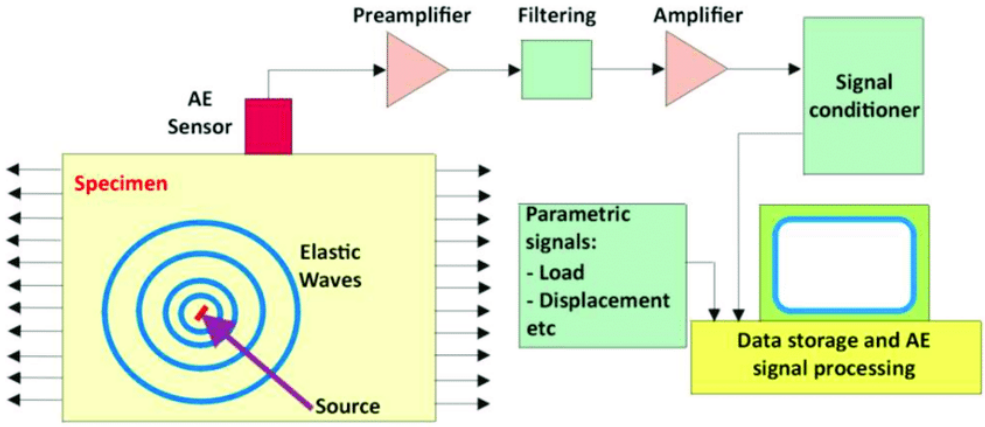

Figure 3: *Overview of acoustic emission capturing and signal acquisition, by Rescalvo et al. [32]*

The repeatability and reproducibility of the AE method has been under some scrutiny, with Khayal and Elmardi [33] having identified two main sources of possible discrepancies between different AE experiments. These are initial geometrical imperfections, which include imperfections in the shape of the specimen and the extent to which the test can be affected by them, and material or constructional imperfections, which relate to pre-existing manufacturing imperfections and to material impurities. To these two categories it is possible to add a third one, namely pre-existing damage within the material, as the AE signals can be affected by the damage state of the specimen. This source of discrepancies has been treated more in detail in the context of fatigue damage accumulation by Kharrat et al. [34].

AE parameters and testing

Acoustic Emissions testing relies on the analysis of the waveforms of signals captured during the testing phase. From these waveforms, certain features can be extracted in order to uniquely identify which damage mechanisms are present during testing [35]. Various parameters can be used in such an analysis, visualized in Figure 4. The AE energy (found as the area under the squared signal envelope), AE counts (found as the number of times the waveform crosses a certain chosen threshold in the positive time direction), time dependent parameters (notably the rise time and duration of the waveform), frequency dependent parameters (such as the peak and average frequencies) and the waveform's amplitude [36].

According to Saeedifar and Zarouchas [35], the most preferred features used to identify damage mechanisms were peak frequency and amplitude. However, the amplitude of the signal is highly dependent on the position of the sensors, due to attenuation of the signal as the wave travels through the material [38, 39]. Therefore, using frequency dependent parameters is preferable, as the properties of the frequency domain seem to be less attenuated over distance than properties of the time domain [35] and thus more invariant to sensor placement. In fact, using a combination of parameters is favored, in order to have a larger amount of data to more accurately uniquely identify damage modes [35]. In essence, from the literature, it can be observed that AE waveform parameters are able to identify quite well which damage mechanisms are present [40].

An often used method to identify the initiation and propagation of damage in the material is the Sentry function, defined as:

$$S_{(x)} = \ln\left(\frac{E_S(x)}{E_a(x)}\right), \tag{1}$$

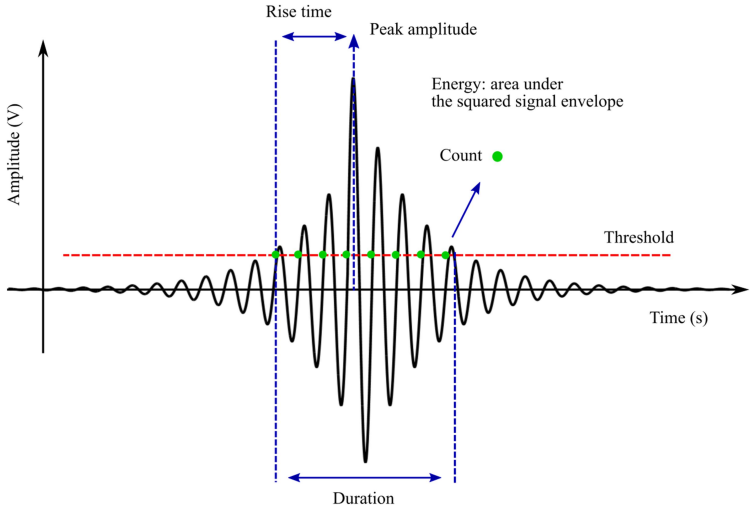

Figure 4: *A typical AE waveform and its most important features [37]*

where $E_S(x)$ is the mechanical energy, $E_a(x)$ is the cumulative AE energy and x is the displacement of the material.

According to Bakhtiary Davijani et al., by looking at the trends in this function the state of the damage can be determined. An increasing trend indicates that no damages occurred or micro crackling in the matrix. Great damages in the material are observed in the function by a sharp drop. A constant trend means that there is a balance between the failures and strengthening mechanisms in the material. Lastly, a gradual decreasing trend indicates that the material cannot carry the loads applied to it anymore [41].

The AE emission waveform also greatly depends on the type of test that is being done. Most authors have chosen to perform tensile static tests on the materials [35]. However, other kind of tests have also been proposed such as double cantilevered beam, compact compression and flexural tests [42], though very few authors have considered compressive testing, itself being a major knowledge gap. Few have also delved into fatigue testing [34, 43, 44], which manifests some differences when compared to static testing, mainly regarding damage accumulation, where one initial damage mechanism will lead to causing another [45].

Association with failure modes

With acoustic emission, according to Saeedifar and Zarouchas, it is possible to distinguish different failure modes by their characteristic signal features. The two most used features to identify the failure type are the peak frequency and the amplitude. The three most common damage modes that can occur in a composite are: matrix cracking, delamination and fiber fracture. Saeedifar and Zarouchas used various characteristic features of the waveforms to better describe these damage modes [35]. Matrix cracking is identified by a low amplitude, a low frequency, a long duration, a long rise time and a large amount of counts in the waveform. Delamination is characterized by an intermediate amplitude, a low frequency and a very long duration. Lastly, fiber fracture is observed as a waveform with a high amplitude, high frequency and a short rise time. Saeedifar and Zarouchas presents his frequency characterization of signals belonging to these damage modes in Figure 5.

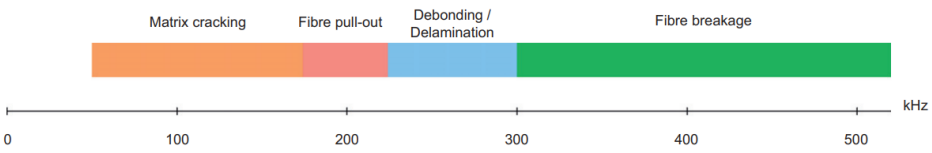

Figure 5: *Peak frequency ranges of different failure modes [46]*

It is important to note that this characterization is not a definitive one, as the methods of analysis and the

testing procedures or tested specimens of various authors lead to different results. In this sense, Saeedifar et al. presented the conflicting in results existing in the field, as shown in Figure 6.

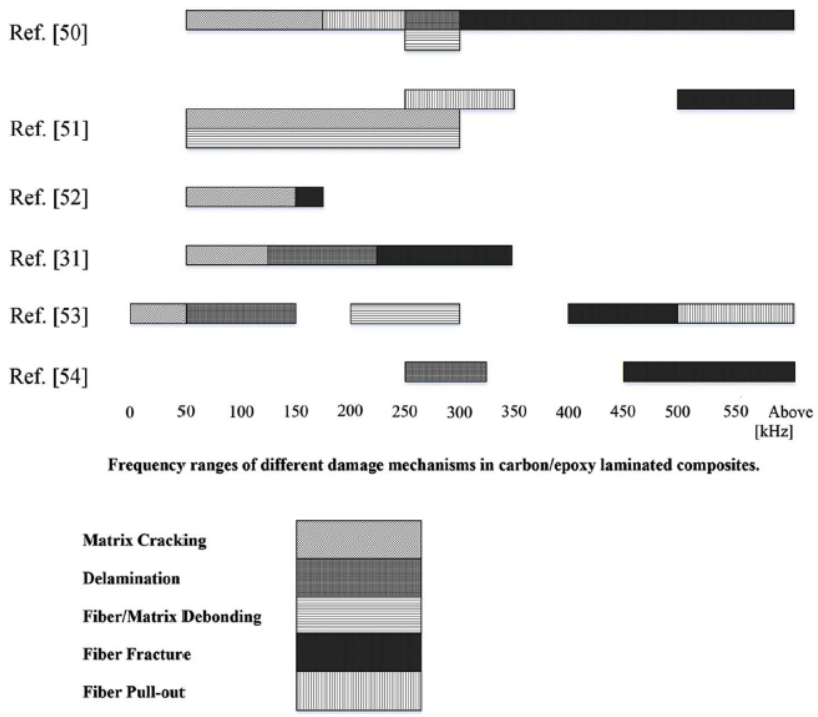

Figure 6: *Frequency ranges of different damage modes as evaluated by multiple authors [47]*

2.4. Data Analysis

Making sense of the experimental results is a fundamental part of the research. The raw data can, of course, not be directly used to make conclusions; processing of the data is necessary to make sense of the results. To do this, various steps must be taken. This ranges from, cleaning up the data (i.e. reducing noise) to clustering results. Each of these steps have different potential methods that can be used having their respective strengths and weaknesses. In this section the different methods are discussed, detailing their applicability and what must be kept in mind when using them.

Pre-processing

From the AE signal, it is possible to extract the different damage mode signals. However, these signals are mixed with noise, that is present within the test, which does not give useful information. To successfully extract the damage mode signals from the original AE signal, the noise must be 'filtered' from the data. This can be achieved using different methods, the most commonly used (applicable to this type of research), being: low-pass filtering, Fast Fourier Transforms, and wavelet filtering [48, 49].

The low pass filtering method artificially reduces measurements above a certain frequency threshold to a 'zero' measurement. This is, however, a quite crude method of reducing noise, as it assumes the noise is of high frequency and takes no regard in possible damage mode signals that may occur in this high frequency range. As such this low-pass filtering method is less suitable for this application as it cannot be assumed that no damage mode signals are present in that high frequency range. Or rather; it is not expected that signals will be produced in that frequency range (as seen from previous research from Saeedifar et al. [50], but it cannot yet be ruled out in this new data.

The Fast Fourier Transform (or FFT) provides a more granular way of reducing the noise signal by removing certain Fourier coefficients from the Fourier-transformed signal. This gives the reducing the noise on a more

dynamic basis. While FFT gives 0 band precision on the filtered frequencies, no temporal elements can be taken into account, due to the Heisenberg uncertainty principle. This is not ideal in cases where there are multiple signals with the same frequency. By sacrificing frequency precision for temporal information combined signals can be more easily be distinguished. This information can be obtained by the wavelet filtering method which is closely related to FFT.

The wavelet filtering method is more versatile than the low pass filtering and FFT method in the sense that it decomposes the signal into signals of varying discrete frequencies.

To achieve this, the 'mother wavelet' (i.e.: the wavelet used for the decomposition) is scaled and translated into multiple wavelets by which the signal is decomposed. In Equation (2) the wavelet scaling function can be found, which explains the method used to scale and translate the mother wavelet.

$$\psi_{a,b}(t) = \frac{1}{\sqrt{a}}\psi\left(\frac{t-b}{a}\right) \tag{2}$$

Where $\psi_{a,b}(t)$ is the scaled wavelet, and a and b are the translation and scaling factors of the wavelet, respectively. The smaller the scaling factor b is, the higher the resolution of the analysis. In that way, multi-resolution analysis can be done, which, as the name suggests, makes it possible to decompose the signal into multiple carrier waves at different frequencies.

The decomposition of the signal with the wavelets is done using a convolution, which is done according to Equation (3):

$$\mathcal{W}_{\psi}(f)(a,b) = \langle f, \psi_{a,b}\rangle = \int_{-\infty}^{\infty} f(t)\overline{\psi}_{a,b}(t)\,dt \tag{3}$$

Where the left hand side is the transformed signal, $f(t)$ is the signal that is to be transformed and $\overline{\psi}_{a,b}(t)$ is the complex conjugate of the wavelet function that is used in the transformation.

The process described above is done in such a way that the original signal can be exactly reconstructed from the decomposed components. This gives the possibility to remove the noise signal, while maintaining the defining parts of the signal wherever in the measured frequency spectrum they may lie. This is of course essential, later on, for the characterization of the damage modes.

Due to the above described reasons, the preferred noise reduction method, and thus the method that will be employed, is the wavelet filtering method. Specifically, asymmetric orthogonal wavelets will be used to preserve the signal energy. The chosen wavelets that have these characteristics are Coiflet and Daubechies wavelets. In the analysis using these wavelets, the scaling order will first be kept low, so as to not preemptively increase low intensity signals (i.e.: noise), and then steadily increased for more significant peaks at points of interest.

To differentiate between noise and other signals, some methods use a noise threshold determination that removes specific wavelet coefficients from the signal. The threshold can be determined using Equation (4):

$$\theta = \tilde{\sigma}\sqrt{2\log(N)} \tag{4}$$

Where $\tilde{\sigma}$ is the estimation of noise variance, and N is the length of the signal [51]. The noise variance, $\tilde{\sigma}$, can be determined from the wavelet coefficients using Equation (5):

$$\tilde{\sigma} = \text{median}(X(k))/0.6745 \tag{5}$$

Where $X(k)$ are wavelet coefficients of the original signal. However, the concern exits that in some cases a signal which principally contains one specific damage mode, will heavily skew the wavelet coefficients. This could lead the method to incorrectly attribute noise to a damage mode signal because it is significantly less dominant in the signal. To mitigate this, values for the coefficient threshold will also be manually configured to more precisely determine if the method is correctly removing only the noise effects.

Should it be necessary, the denoised signal can be reconstructed using the inverse continuous wavelet transform [49], as described in Equation (6):

$$f(t) = \frac{1}{C_\psi} \int_{-\infty}^{\infty} \int_{-\infty}^{\infty} \mathcal{W}_\psi(f)(a,b)\psi_{a,b}(t) \frac{1}{a^2} \, dadb \tag{6}$$

Where $f(t)$ is the reconstructed signal, and C_ψ can be determined with Equation (7):

$$C_\psi = \int_{-\infty}^{\infty} \frac{|\hat{\psi}(\omega)|^2}{|\omega|} \, d\omega \tag{7}$$

Where $\hat{\psi}(\omega)$ is the Fourier transformed wavelet function, and ω is the angular frequency variable used in the Fourier domain.

Feature Extraction

From this now pre-processed data, feature extraction can take place. As the signal now contains far less noise due to the pre-processing, it is less likely that damage modes are incorrectly attributed to the effects of noise. Various methods can be used to make sure the correct, or different features, are extracted. The suitable methods can be found in the following Section 4.4.

Clustering cannot be applied to the AE signals directly. Instead, the complex waveform has to be transformed in a representation that is amenable to analysis. This is done by extracting features, which are characteristics of the measurements that possibly encode the damage mode in some way. These features range from basic properties of the time and frequency domain to results from advanced transformations.

An example of a typical AE waveform in time domain is shown in Figure 4. The features are described by Saeedifar and Zarouchas [35]. The peak amplitude and energy (area under the squared signal) can be found directly. After defining a threshold, the number of counts (upward crossings of the threshold), rise time and duration can be computed. In the frequency domain, the peak frequency and central frequency are useful features, especially since properties of the frequency domain are less attenuated over distance than properties of the time domain.

The frequency components can be obtained from the time domain signal with multiple methods. The two most common ones are presented by Brunton and Kutz [49]. Fourier transform decomposes the signal into sine and cosine functions at a range of frequencies. These basis functions extend towards infinity in time and thus do not convey locality, i.e. where sections involving a certain frequency occur. The wavelet transform generalizes the concept of decomposition to other basis functions which may be locally confined. By scaling and translating a wavelet, the signal can be represented in a hierarchy of increasing resolution and decreasing time span to enable multi-resolution analysis. From wavelet transform results, the energy in certain frequency bands can be computed and used as feature. An adapted version called the empirical wavelet transform generates wavelets based on the data [52].

Autoencoders are a special case of artificial neural networks which are useful for dimensionality reduction but also feature learning [53]. The network is trained to reconstruct the input, but a bottleneck is present to retain only the most salient properties. After the network has been trained, the activations in the bottleneck layer can be used as features.

Of all the features presented, peak frequency and peak amplitude are the most useful features in damage identification, but using multiple features gives higher confidence in the prediction [35].

Dimensionality Reduction

All features presented in the previous section lead to a high-dimensional feature space. In this case, distance metrics used in clustering are not clearly defined anymore and thus lose meaning [53]. This is also known as the ”curse of dimensionality”. Dimensionality reduction techniques can alleviate this issue by transforming features into a lower-dimensional space while retaining the most meaningful information [54].

The most widely used method for dimensionality reduction is Principle Component Analysis (or PCA). The PCA method aims to reduce large quantities of data into the most meaningful components that capture the most variance in the data set.[49] This is especially useful in cases that the data contains large amounts of factors (in this case frequencies) that do not necessarily correlate with any damage modes, or at the most are very weak indicators of these. The main advantage of this technique is that it is an unsupervised machine learning algorithm, meaning that no prior knowledge is needed about the labels of the data points.

The main concern with the PCA method of reducing the data is that it is quite sensitive to outliers in the data set. Incorrect measurements or corrupted data could lead to principle components that incorrectly describe the original data. To prevent outliers from significantly altering the principal components, an altered version of PCA can be employed: Robust PCA. This method significantly reduces the effect of outliers, thus keeping the principal components as accurate as possible.[55]

Clustering

Once features have been extracted and optimized, the damage mode can be identified. While this is a classification task, supervised classification methods cannot be used since no labels are available. Labeling requires microscope or camera imaging with manual label assignment, which is a time-intensive task. Therefore, unsupervised clustering methods are more practical, requiring no a priori knowledge of the damage mode. A small set of labeled measurements can then be used for validation and identifying the damage mode of each cluster.

Several clustering methods are commonly used in machine learning:

K-Means : iteratively assign data points to cluster based on distance to cluster centroid, then update cluster centroid as mean of assigned data points, convergence is dependent on initial centroids

Genetic K-Means : an improved version of the K-Means version helping with convergence to global optimum

Fuzzy C-Means : similar to K-Means, but membership of each data point is continuous between 0 and 1 instead of binary

Self Organizing Map (SOM) : a type of neural network that fits a grid to the data points which can be used for partitioning

Hierarchical clustering : creates a cluster tree (dendogram), can be either divisive (top-down) or agglomerative (bottom up); Divisive methods follows these steps:

1. Each data is considered a cluster and cluster distance is calculated
2. Merging of the closest clusters
3. Calculation of new cluster distances
4. Iteration

The number of clusters must be set manually for some of these methods. To determine the optimal number of clusters, there is a number of criteria. The Davies–Bouldin criterion minimizes the ratio of within-cluster distance to between-cluster distance. The silhouette criterion maximizes the similarity between points of the same cluster. The Gap and Calinski–Harabasz criteria may also be useful.

3. Research question, aims and objectives

The remaining part of the AE2223-I Test, Analysis & Simulation project will focus on the data analysis and answering our main research question, namely:

> Which damage modes of CFRP can be accurately identified and differentiated using analysis of acoustic emission recordings?

By answering this question we aim to identify the different damage modes of CFRP under both static and fatigue compression loads using AE. Moreover, an analysis pipeline will be developed to efficiently identify the damage modes. Additionally, to answer the main research question, some sub-questions will need to be answered along the way. These sub-questions are:

1. What unsupervised clustering technique are we using?
2. What is the optimal number of clusters?
3. Can AE be a reliable indicator of damage mode onset in CFRP?
4. How can AE data be clustered such that clear damage mode identification within CFRP is possible?
5. What waveform parameters give the most insight into the damage modes of CFRP after CAI testing?
6. Can AE be used alongside other damage detecting methods to measure the onset of damage modes?
7. How well do the damage modes of the clusters compare to the force-displacement data?
8. Is it possible to differentiate between damage modes when they occur at the same time using AE?
9. Which features identify most with a damage mode/cluster?
10. What can we learn from the analysis of AE between static and fatigue tests?

With these sub-questions we will get closer to answering our main research question, additionally these questions are answered by reaching certain intermediate goals and aims. The goals of the sub-questions are, respectively:

1. Determine the unsupervised clustering method with the best resulting clusters for further analysis.
2. Determine a method that uses similarity based indicators to identify the optimum number of clusters for a specific data set.
3. Investigate and validate our data analysis method on various data set in order to establish the reliability of the method.
4. To cluster AE data as structured as possible.
5. Determine the different damage modes present after CAI.
6. Determine the different damage modes that actually occur during testing and how to link them with the clusters.
7. Determine whether the identified clusters are correct.
8. Differentiate the damage modes with the data clusters obtained by only AE.
9. To remove unnecessary computations spent on investigating less useful features.
10. Being able to compare both loading types and their results.

By completing all the listed goals, we will get closer to our main objective, which is to identify the damage modes present under compressive loads in both static and fatigue loading, by developing an efficient analysis pipeline, based upon AE measurements. This objective was chosen, as there is a lack of physical understanding of the damage modes and their propagation in CFRPs, due to the current focus on making predictions of damage and failure. Moreover, after answering the main research question, and having been able to link clusters to certain damage modes, the results will hopefully fill the knowledge gap of the underlying physics.

4. Methodology

Identifying and differentiating damage modes in AE recordings will require experiments and subsequent analysis. This section explains how the answer will be found from experimental results using a data analysis pipeline.

4.1. Pipeline overview

The data analysis pipeline is shown in Figure 7. The pipeline takes AE waveforms as input and it outputs the identified damage modes. In between, there are 5 stages: pre-processing, feature extraction, dimensionality reduction, clustering, and evaluation. While many different techniques could have been used in each stage, the best ones for this problem have been selected based on the literature review.

The **pre-processing** stage aims to reduce noise in the raw waveform. A band pass filter of $90\,\mathrm{kHz}$ to $900\,\mathrm{kHz}$ is already applied to this waveform based on the characteristics of the sensor. Therefore, no further low-pass or high-pass filter is applied. Instead, wavelet filtering is employed to give maximum flexibility in separating signal and noise in the time and frequency domain.

Based on the filtered waveform, **features are extracted** in the next stage. A wide range of features have been selected so that the damage mode is accurately recorded. While this results in a very high-dimensional feature space, dimensionality reduction will reduce the dimension to a magnitude amenable for clustering. A major contributor to the many dimensions is the feature ”first n samples”. If this feature does not show large contributions in the PCA, it may be removed.

Features are extracted from the waveform in four ways. Firstly, basic AE waveform properties like peak amplitude and duration can be found directly. The ”first n samples” provide a baseline against which the effectiveness of other features can be compared. Secondly, a Fourier transform will give frequency information details. Thus, peak amplitude and peak frequency, which were found to be the most significant features are presented. Thirdly, an autoencoder neural network (or possibly multiple stacked ones) is trained to encode an efficient representation of the waveform. The activations of the hidden bottleneck layer are then used as features. Finally, multi-resolution analysis based on wavelets will enhance the Fourier transform features with time information. Specifically, the energy of certain frequency bands in different sections of the waveform is extracted. After feature extraction, they are normalized to ensure equal weighting of all features used in the PCA.

PCA, or possibly robust PCA, then **reduces the dimension** of the feature space by finding the principal components. Reducing the dimensionality is necessary for distance metrics in clustering algorithms to have meaning. PCA was chosen over LDA or another autoencoder because implementations are widely available and do not require labeled data.

Clustering will then group similar examples, ideally by their damage mode. Four clustering methods are tested and compared. Firstly, k-means provides a baseline as a simple and commonly used algorithm. Secondly, fuzzy c-means is used to see if the small modification of allowing continuous, instead of, binary cluster assignment is useful. Thirdly, hierarchical clustering is tested, which was found to be the most reliable method in literature. Finally, a self-organizing map was chosen to see if advanced neural network-based machine learning algorithms can outperform classic algorithmic methods. The optimal number of clusters for k-means, fuzzy c-means and hierarchical clustering is determined by a voting scheme between

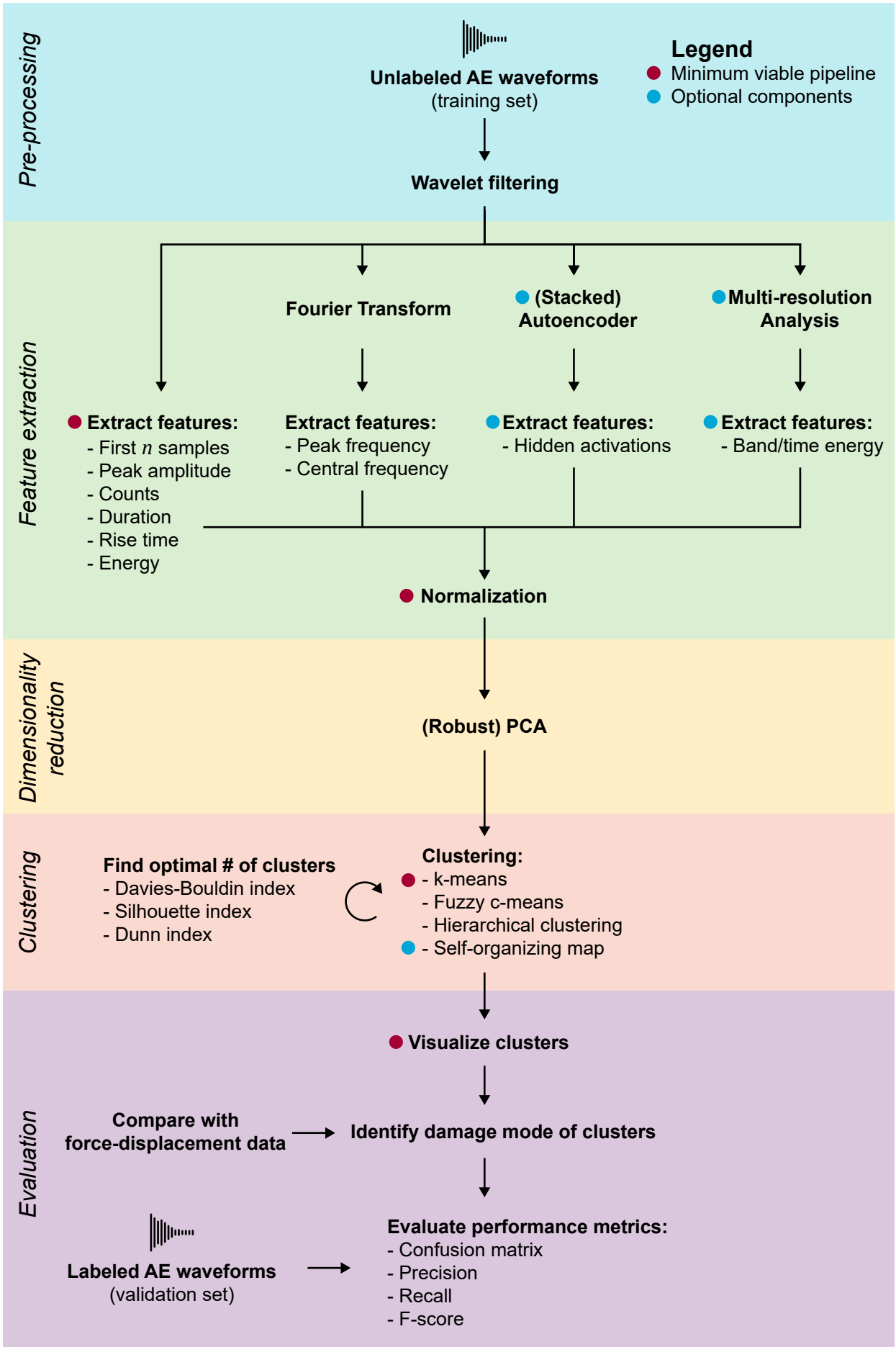

Figure 7: *A flow diagram of the complete data analysis pipeline. The goal is the identification of the damage modes based on AE measurement. The pipeline consists of 5 stages, with feature extraction and clustering being the most important. A minimum viable pipeline is indicated by red dots, while optional components are marked by blue dots.*

multiple indices.

Once clusters have been identified, they can be visualized and compared with available force-displacement data to **identify the damage mode** of each cluster. This will allow classification despite using unsupervised clustering. While visualization is very helpful in the development process to get visual insight into the pipeline, the presentation of clusters in the high-dimensional feature space is challenging and remains a problem to be solved. Finally, the performance of the pipeline can be evaluated using classification metrics and a confusion matrix.

The pipeline has to support two modes: training and prediction. During *training*, a large number of examples called the *training set* are presented to the pipeline to find patterns. Some components do not require such training (e.g. Fourier transform and direct features), since they are stateless and regard examples individually. However, most components will require fitting as part of the machine learning process. Most notably, this includes the clustering algorithms, PCA and autoencoder, but also the threshold and individual parameters in normalization and wavelet filtering. After training on the whole training set, the pipeline can be used for *prediction* of the damage mode of individual examples. Additionally, prediction for a labeled *validation set* leads to quantitative performance metrics such as precision and recall.

4.2. Development of the pipeline

The development of the pipeline can be very modular and parallel, since each component can be developed independently once a common interface is defined. Unit testing can be used to test the components and give confidence in their functionality and correctness, which then extends to the whole pipeline.

At first, a minimum viable version of the pipeline will be developed, containing only a single component of each stage. These components are marked with a red dot in Figure 7. While this pipeline will likely not give accurate results, it serves as a foundation that can be extended easily once the more advanced components are completed. Components marked with a blue dot are optional, meaning that they may be interesting to investigate and may increase prediction accuracy, but not regarded as crucial for successful prediction.

4.3. Pre-processing

The raw data from the experiment must be pre-processed before it can be used in in the data processing pipeline. To achieve this, wavelet filtering will be employed.

Wavelet filtering can be done in various ways, different wavelet families exist with various applications and within those, varying strengths and weaknesses. For the kind of data in this research, orthogonal wavelets are necessary to preserve the signal energy. The wavelets that have these characteristics, and are applicable to this type of data, are Coiflet and Daubechies wavelets.

In this analysis, the scaling order will first be kept low (e.g.: a scaling order of 2, 3), so as to not preemptively increase low intensity signals, and then steadily increased for more significant peaks at points of interest. Furthermore the translation factor of the wavelet transformation must be configured for the desired resolution as can be found in Equation (2) in Section 2.4. In some cases this determination will be executed by the method from the code packages used in the analysis program.

Furthermore, the threshold for the wavelet coefficients must be determined to indicate where the cutoff for the wavelet coefficient values should lie. According to Donoho and Johnstone [51], the best estimation for the noise threshold level can be determined using the method described in Section 2.4.1. However, the concern exits that in some cases a signal which principally contains one specific damage mode, will heavily skew the wavelet coefficients. This could lead the method to incorrectly attribute noise to a damage mode signal because it is significantly less dominant in the signal. To mitigate this, values for the coefficient threshold will also be manually configured to more precisely determine if the method is correctly removing only the noise effects.

From this, now, pre-processed data, feature extraction can take place. A necessary step before the data points can be clustered. As the signal now contains far less noise due to the pre-processing, it is less likely that damage modes are incorrectly attributed to the effects of noise. Various techniques can be used to make sure the correct, or different features are extracted. The suitable methods can be found in the following Section 4.4.

4.4. Feature Extraction

Features are extracted from the filtered waveform in four components: direct extraction, Fourier transform, an autoencoder and multi-resolution analysis. These can be developed and executed in parallel. Some components have adjustable parameters, for which the optimal value needs to be found manually or mathematically.

For direct extraction, the main parameter is the threshold, shown in Figure 4. The threshold determines the amplitude distinguishing the actual signal from noise. It is relevant for counts, duration and rise time. A value for the threshold will be found by experimentation and inspection. For the ”first n samples” feature, the number n will by found in the same way, with the knowledge that most of the useful information is concentrated near the start of the waveform.

Fourier transform is straightforward and FFT implementations are found in widely available packages. The central frequency can be found as the amplitude-weighted average of frequencies.

The autoencoder is a type of neural network and will be implemented in the PyTorch package. All samples of the filtered waveform will be given as input and used for reconstruction. There are many parameters to vary. The number of hidden layers and size of these layers will have a large impact, especially the size of the bottleneck layer, which corresponds to the number of features from this feature extractor. Apart from that, many hyperparameters such as training epochs, learning rate, and optimizer function can be chosen, but time constraints will likely not allow detailed hyperparameter optimization.

Since the multi-resolution analysis is based on the wavelet transform, much of the same considerations apply here as for wavelet filtering, described in the previous subsection. The choice of mother wavelet and number of levels will have the most influence. Whether a fixed wavelet family will be used, or it will be determined dynamically using the empirical wavelet transform, is still to be determined.

4.5. Dimensionality Reduction

All features presented in the previous section lead to a high-dimensional feature space. Dimensionality reduction techniques can alleviate this issue by transforming features into a lower-dimensional space while retaining the most meaningful information [54].

The PCA method aims to reduce large quantities of data into the most meaningful components that capture the most variance in the data set [49]. The main concern with the PCA method of reducing the data is that it is quite sensitive to outliers in the measurements. Therefore, an altered version of PCA will be employed: Robust PCA, as described in Candès et al. [55]. This method significantly reduces the effect of outliers, thus keeping the principal components as accurate as possible.

This will have reduced the data into its principle components. From these components that make up the variance of the data set, it is preferable to have a low amount of components capturing a high amount of variance. This is of course not always achievable, as there is the possibility of a large amount of principle components each only capturing a modest amount of variance. Therefore, a trade-off must be made between captured variance and dimensionality. After inspection, a decision will be made on how many components will be used for clustering.

4.6. Clustering Data Points

From the now lower dimensional feature space, clustering can take place. The goal is to divide the data points into at least three clusters, each representing a damage mode. This is determined by using the euclidean distance and a voting scheme based on indices.

The four main methods used for clustering are k-means, Fuzzy c-means, Hierarchical Clustering, and SOMs (self organizing maps). The former three can be easily implemented using the SciKit Learn package. The k-means method requires minimal input data, limited mainly to the number of clusters k it must divide the data into. Other parameters determine how many tries the method gets and other tolerances.

Fuzzy c-means requires, again, the number of clusters k the data should be divided into, as well as an m parameter. This m parameter is generally found empirically within the range of 1.5 to 3 [56]. Also with this method other parameters can be adjusted for tolerances within the method.

Hierarchical clustering again requires the number of clusters k to divide the data. It also requires the affinity, in this case euclidean, and the linkage criterion. This criterion can be chosen from, ward, average, complete, and single. 'Ward' minimizes the variance of the clusters being merged, 'average' uses the average of the distances of each observation of the two sets, 'complete' uses the maximum distances between all observations of the two sets, and uses the minimum of the distances between all observations of the two sets. This criterion will have to be determined after examining the data more closely, however, we expect 'ward' linkage to provide the best clustering results for the data from this research.

Self-organizing maps are a type of neural network for which no package exists. Therefore, a custom implementation in PyTorch is required. Just as for the autoencoder, the network structure and hyperparameters can be varied, and optimal values need to be found experimentally. In addition, a neighborhood function needs to be chosen.

The number of clusters k needs to be set a priori for k-means, fuzzy c-means and hierarchical clustering. Multiple increasing values will be tried, starting with 3 clusters since that is the expected number of main damage modes. How optimal a certain k is will be evaluated using the Davies-Bouldin index, the Silhouette index and the Dunn index. These indexes will cast voting points, and the cluster with the most points is the optimal one. This voting scheme is used by Liu et al. [57].

Visualization of High-dimensional clusters

While clustering is of a pure mathematical nature, it is often useful for a human interpreter to visualize the data as to give meaning to the results. For data that is of low dimension, it is trivial to visualize in a two- or three-dimensional space. However, with high dimensional data is quickly becomes quite challenging to successfully convey the desired information on the dependency of the data points in a way that is interpretable by humans. Thus, creative methods must be used to successfully convey the desired information.

As the data from this research may still be of high dimension, even after dimensionality reduction, a method to visualize the data must be used. A special package, Napari, written for Python exists to do this, and so it will be applied in the program. However, this package is still in alpha phase and may not provide the required results. Another method that can be used is plotting the data in three dimensions and varying the marker in shape, color, and size, indicating the different clusters.

4.7. Identification of Damage Mode of Clusters

Once clusters have been found, they have to be assigned to a damage mode in order to enable classification. The fundamental approach is to find the damage mode for some examples, either by visual/microscopic inspection as for examples in the validation set, or by comparison with the force-displacement data, looking for the mode's signature. Then, these examples are run through the pipeline to see to which cluster they are assigned. Ideally, all examples of one damage mode are assigned to the same cluster. Then, the damage mode of each cluster has been identified with high confidence.

At this point, the research question can be answered qualitatively. However, a quantitative evaluation based on a validation set and metrics will give more credibility to the results. These will be discussed in Section 6.

5. Experimental setup

To obtain the required data, static and fatigue compression after impact tests will be run. First Section 5.1 will describe the lay-up and geometry of the carbon fiber reinforced polymer test samples, then Section 5.2 explains the impact setup, Section 5.3 will go over the static compression test setup, and finally Section 5.4 describes the fatigue test.

5.1. Test sample

The sample that will be used for testing, is a $100\text{x}150$mm, rectangular CFRP sheet. The sheet consists of 32 layers, with a quasi-isotropic $[45, 0, -45, 90]_{4,s}$ layup. Thermoset epoxy resin is used as a matrix, and the average thickness after curing is 5.15mm.

5.2. Impact setup

Before testing for damage modes in compression the sample must first be damaged. The initial part of the test will be performed using a drop-weight impact event. This test will follow the standard test method D7136/D7136M-20 for drop-weight impacts on fiber-polymer composites [58].

Initially the sample will be secured in a support fixture. It is placed on a fixture base of at least $300\text{x}300$mm with a $75\text{x}125$mm cut-out below the sample and secured by four rubber-tipped clamps shown in Figure 8b [58, p. 3]. The clamps will secure the sample with minimum clamping force 25mm from the specimen edge.

The support fixture will then be placed at the bottom of an impactor device and held up by a 300mm long support in each corner. Guiding rungs above the the support fixture will hold the drop tube with the impactor at one end. This setup is shown in Figure 9 [58]. Either by hand or machine, the drop tube will be set and held at the selected drop height. This will be selected based on the desired impact energy; the impact energy is defined in Equation (8).

$$E = C_E \cdot h \tag{8}$$

Where E is the impact energy, C_E is the ratio of impact energy to specimen thickness and h is the specimen thickness. The impact energy ratio target for the sample specified in Section 5.1 is $6 \cdot 7$J/mm. This will be used to determine the drop height; defined in Equation (9).

$$H = \frac{E}{m_d \cdot g_0} \tag{9}$$

Where H is the drop height, g_0 is the gravitational acceleration at test-level and m_d is the mass of the impactor. Applying these equations for the sample defined in Section 5.1 will require the drop height to be set to $0 \cdot 7328$m. All the elements on the impactor tube shall be rigidly attached to minimize resonance on impact. When dropped, an out-of-plane impact will hit the sample. For the specimen mentioned in Section 5.1 the point of impact will be centered as shown in Figure 8a [58].

The impact is performed using a hemispherical impactor, with a radius of 8mm and mass of $4 \cdot 8$kg, which will result in a high-mass, low-velocity type impact. This impact will occur once without rebound which can be prevented by either a specific mechanism or quickly sliding a piece of material between the sample and the impactor.

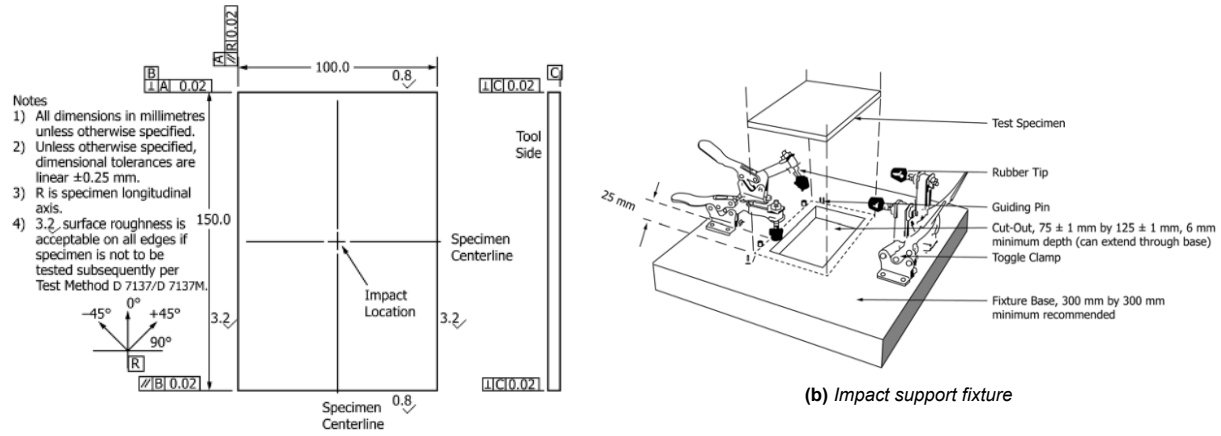

(a) *Impact location on sample*

(b) *Impact support fixture*

Figure 8: *Impact sample setup [58]*

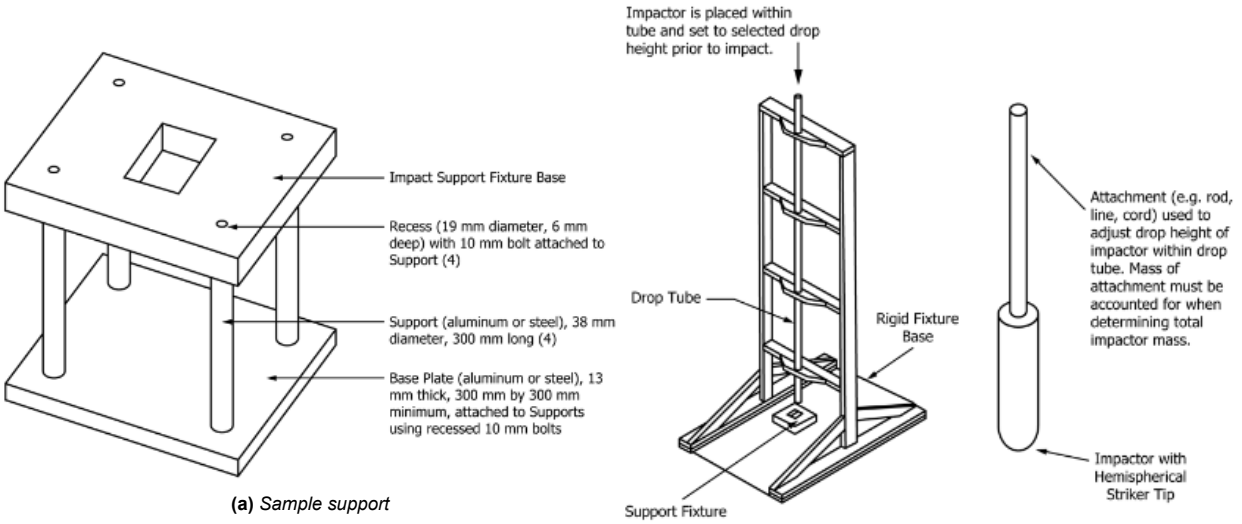

(a) *Sample support*

(b) *Impact device*

Figure 9: *Impact device setup [58]*

After the impact it will also be possible to utilize a velocity detection mechanism to calculate the actual impact energy. This is defined by Equation (10).

$$E_{actual} = \frac{m_d \cdot v^2}{2} \tag{10}$$

Where v is the impact velocity. The impact will result in the initiation of damage modes in the sample. These damage modes will be made up of BVID type damage modes due to the use of a hemispherical impactor and low-velocity impact. Additionally, since this is mainly part of the preparation for further testing, no in-depth data needs to be recorded.

5.3. Static CAI testing

For the static CAI tests, international standard D7137/D7137M − 17 will be followed, so that the results can be easily compared to experiments performed by other research groups [59]. The test sample, as described in Section 5.1, will have been damaged by an out-of-plane impact, as in Section 5.2. The specimen will then be mounted in a clamp, such that the $0°$ direction is lined up with the compressive force, as can be

seen in Figure 10 below:

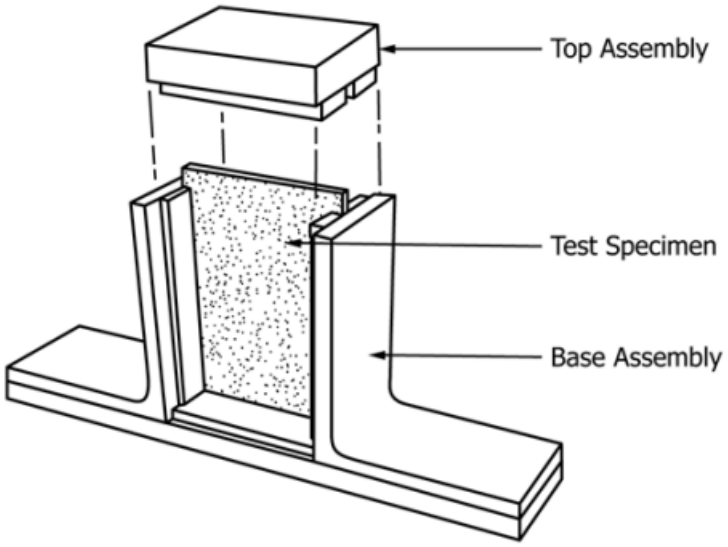

Figure 10: *Schematic of the support fixture for CAI testing [59]*

This clamp also supports the plate along the sides, to prevent global buckling during compression. The clamp is mounted in a compressing machine, that records the force exerted on the sample and the displacement.

Two piezoelectric AE-sensors will be mounted on the test-specimen, which will record the vibrations at the surface of the sample at frequencies between $100 - 900$kHz [60]. The sensor data is then passed to a pre-amplifier, before some filtering is done by selecting the desired frequency range. This data is then passed through another amplifier, after which the data can be processed further for analysis.

Once the test starts, the compressive load will slowly be increased. As damages starts to occur, these signals will be picked up by the AE-sensors and will be stored alongside the force and displacement data. The compressive load will then be increased until failure of the test specimen. The sensor data will then be analyzed to identify the types of damage that occurred at which time.

5.4. Fatigue testing

The fatigue test will use the same test setup as the static compression test in Section 5.3. However, instead of increasing the load until failure, in this test the specimen will be loaded cyclically up to a lower load level than the static test. Two separate test will be performed, one where the load varies between 6-60$\%$ of the static CAI strength, and another where it varies between 7.5-75$\%$. For both of these tests, the loading will be varied sinusoidally at a frequency of 3Hz. These loading cycles will continue until the samples fail. As fatigue tests can run from hundreds to millions of cycles, depending on the load level, this will result in a lot of data. To make analysis of this data more manageable, only smaller intervals around certain cycle numbers will be analyzed.

6. Validation

In order to conclude if the data analysis performed is correct, a method for validation of the results is required. In this way it would be possible, based on the validation criteria selected, to compare and assess the accuracy of each path within the pipeline. Thus, the most accurate and successful data analysis method can be selected.

Firstly, there is a need for some validation criteria that describe the accuracy of classification of the various damage modes studied. As the method of clustering the data points is unsupervised, a correct, labeled data set is needed as a comparison standard. One way to visualize the accuracy of classification of each damage mode is to use a confusion matrix. As the name suggests, the confusion matrix is a square grid that shows, usually as a percentage, the amount of times each damage mode was either correctly, or wrongly, predicted. Each row represents the true label of the data points, while each column is giving the predicted label. Thus, the places of the matrix that lay on the main diagonal represent the amount of true predictions, while the other positions are erroneous predictions. A confusion matrix example is provided in Figure 11. It is worth to mention that the ideal case, without any error in the prediction, is to have a confusion matrix identical to the identity matrix.

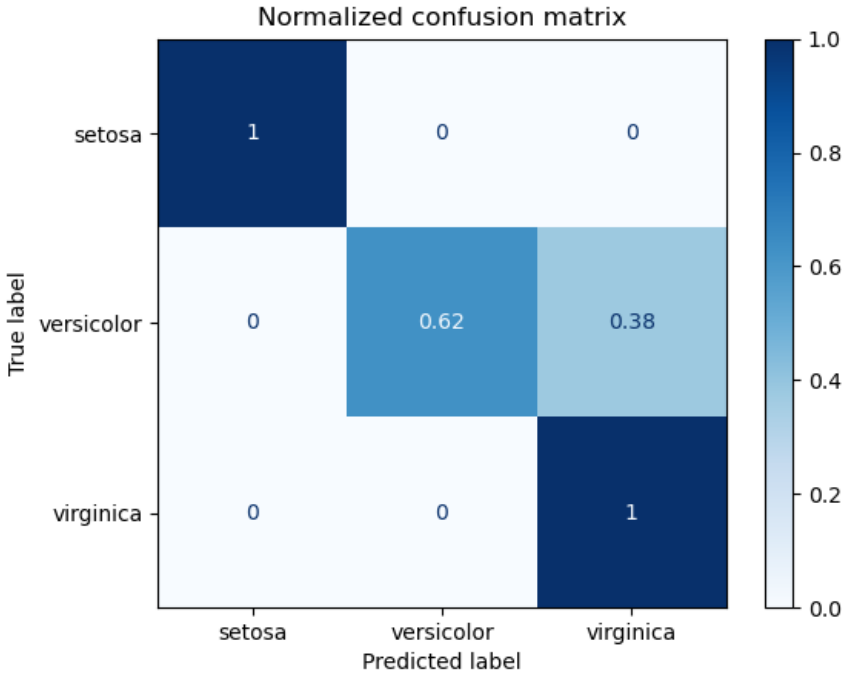

Figure 11: *Normalized confusion matrix for a predictive space of three elements*

Another metric for validity assessment of a predictive algorithm is the precision of its guesses. Precision measures the number of correct positive predictions out of all the predictions. A simple equation for the precision of a predictive model is given in Equation (11), usually given as a percentage. Thus, the precision metric can take values between 0, meaning that the damage modes were never correctly identified, and 1, meaning a perfect prediction.

$$Precision = \frac{TruePositives}{TruePositives + FalsePositives} \tag{11}$$

Similarly to precision, recall also measures the amount of positive correct predictions, but out of all the positive predictions that could have been made, instead of the positive guesses that were made. The explicit formula for recall is given as Equation (12). Again, we can see that the recall can take values between 0 and 1, making better predictions has a recall score closer to 1.

$$Recall = \frac{TruePositives}{TruePositives + FalseNegatives} \tag{12}$$

It is important to note here that maximizing precision and recall have different purposes, namely maximizing precision leads to minimizing the amount of false positives, while maximizing recall will minimize the amount of false negatives. Thus, a prediction algorithm can have excellent precision, but poor recall, or vice-versa. A better validation metric that combines these two parameters is the F score, computed as shown in Equation (13). This new indicator balances both precision and recall in order to give an overview to the validity of the prediction, which is why it is the most commonly used metric to quantify validity.

$$F_{score} = \frac{2 \cdot Precision \cdot Recall}{Precision + Recall} \tag{13}$$

Secondly, validation of the clustering method should also take place. A method commonly used to validate k-means clustering is the Silhouette analysis. This is an internal validation method that estimates the average distance between clusters as well as measuring how well an observation is clustered. This method is comprised of analyzing the silhouette width, which can vary from -1 to 1, to determine whether an observation is well clustered or not. Larger values (close to one) mean that the observations are well clustered, values close to zero lie between two clusters, and values close to negative one means that observations are probably placed in the wrong cluster. This metric of silhouette width can be calculated with Equation (14):

$$S_i = \frac{b_i - a_i}{max(a_i, b_i)}, \tag{14}$$

where the index i refers to a certain observation, a_i is the average dissimilarity between i and all other points in the cluster, and b_i is the dissimilarity between i and its neighboring cluster.

These validation methods will be able to give a definitive answer to our main research question: ”Which damage modes of CFRP can be accurately identified and differentiated using analysis of acoustic emission recordings?”, as stated in Section 3. The aforementioned question focuses on two main parts, accurate identification and correct differentiation of damage modes.The accuracy of damage mode identification will be tested and assured by the metrics of prediction accuracy, while the differentiation of damage modes will be assessed based on the clustering method validation process. Thus, the overall validity of the method will be able to confirm if and to what extent the goal of the research has been met.

7. Project planning and Gantt chart

To complete our objective of identifying the damage modes present under compressive loads in both static and fatigue loading, by developing an efficient analysis pipeline, based upon AE measurements, a plan is needed. A way to visualize the logistics of all the required work, is by utilizing a Gantt chart. This can be based on all the goals mentioned in Section 3 and the various steps of the pipeline of Section 4. Moreover, a Gantt chart allows for visible review points like milestones and deliverable [61]. For this project, two four-hour sessions are planned each week, on both Wednesday and Friday morning from 08:45 to 12:30, with the exception of week 13, 14 and 15 and some holidays in the fourth quarter. Based upon the pipeline from Section 4 and the goals of Section 3 the following eight work packages were identified:

1. Pre-processing of data (wavelet filter, low pass filter, FFT)
2. Feature extraction using Fourier transform/ wavelet transform + n first samples
3. Dimensionality reduction using PCA
4. Clustering analysis + finding optimal number of clusters
5. Cluster visualization
6. Identification of damage modes corresponding to a certain cluster
7. Comparison with force-displacement data and images

8. Evaluating performance metrics of the pipeline

Additionally, some deadlines will need to be added. These are the three mandatory group deadlines after the fourth of March 2022 for the AE2223-I Test, Analysis & Simulation course:

1. Assignment: Introduction & Methods of Scientific Article [22-4-2022]
2. Assignment: Finish Draft version of Scientific Article [11-5-2022]
3. Assignment: Finish Final version of Scientific Article [10-6-2022]

Based on these work packages, deadlines and planned project sessions, a Gantt chart for this research plan was made using Instagantt and can be seen in Figure 12. A larger version of this chart, including start and end dates for every task can be found in Figure 13 in Appendix A. The lock icons visible in the Gantt chart show the deadlines that are hard deadlines. An additional soft deadline for a finished version 1.0 of the pipeline is included on the 29th of April. The dates highlighted in yellow are non-working days due to exams. The time after the reflection and evaluation is reserved for writing and reporting our results for the final version of the article.

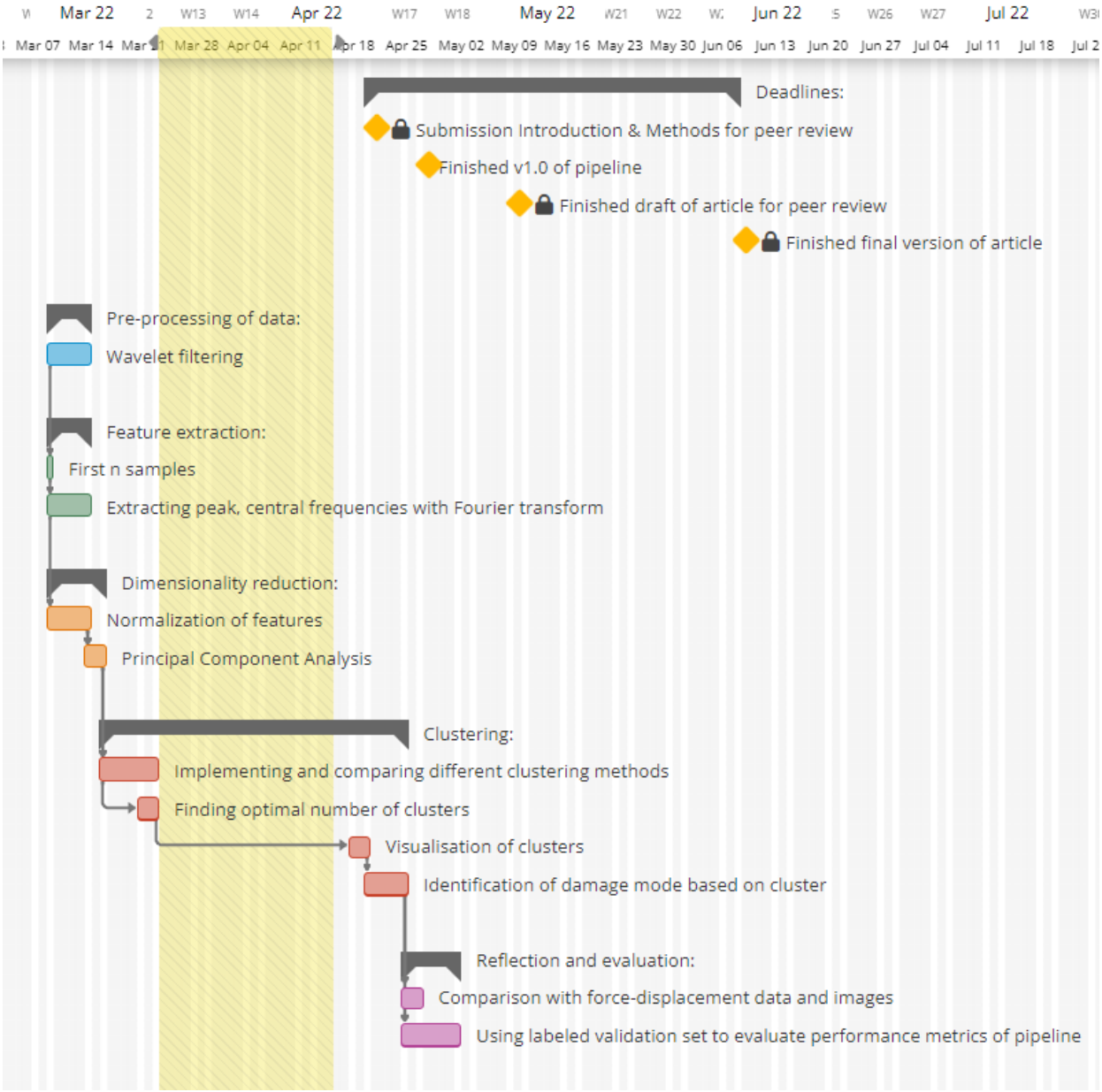

Figure 12: *Gantt chart based on the work packages, made using Instagantt.*

8. Conclusions

The main objective of the research is to differentiate and identify the damage modes present in CFRP, both under static and fatigue loading, based on acoustic emission measurements. This identification is aimed to be achieved by developing an analysis method. This analysis method will be able to filter and cluster the measurements and connect these different clusters to specific damage modes which are present in the material. Another goal of this research is to determine which methods do this most efficiently.

Currently, there is no real physical understanding of damage modes and their propagation in CFRPs under compression after impact, only rough predictions of damage and failure can be made. So this research aims to fill this knowledge gap by developing an analysis method through which measurements from acoustic emission can be given physical meaning. The physical meaning of the measurements can be used to attain some physical understanding of which damage modes are present and their propagation in CFRPs under both static and fatigue compression loads. Furthermore, current testing methods are limited either because they can not detect all damage modes or because they are destructive which is not ideal. The testing method which will be used in this research, acoustic emission, has the potential to address these problems. There has been some research into acoustic emission but most of these chose to perform tensile static tests on the materials, very few perform compressive static tests [35]. Thus, another knowledge gap that our research is aiming to fill is whether acoustic emission can also be used for damage mode detection and identification during compressive and fatigue loading testing.

The data which will be used in the data analysis is gathered during two different experiments. The specimen to be used is a 100x150 mm, rectangular CFRP sheet. Before this specimen is tested it will undergo a drop weight impact. This impact is created by an impactor device which is able to apply a controllable high-mass, low-velocity and out-of-plane impact.

After the specimen has undergone this impact it will undergo either static CAI testing or fatigue testing. For the static CAI testing the specimen will be clamped on by four clamps. The clamped specimen will then be mounted in a compressing machine. The force exerted and the displacement will be continuously recorded. The load will be increased until failure of the specimen. During the experiment, two AE sensors, which will be mounted on the specimen, will record the vibrations in the specimen. These vibrations will be amplified and filtered after which the data is ready for analysis. For the fatigue test the same test setup will be used. In this test the specimen will be loaded cyclically up to a lower load level. The specimens will be tested at two different load levels. These loads will be applied sinusoidally. The cycles will continue until the specimens fails. The data acquiring will be done in the same way as during the CAI test.

The pipeline which will transform the AE data into identified damage modes will consist of five stages: pre-processing, feature extraction, dimensionality reduction, clustering and evaluation. During pre-processing wavelet filtering is used. Features are then extracted from the waveform in four ways. Firstly, basic properties like peak amplitude and duration can be found directly. Secondly, a Fourier transform will be used to find the peak frequency. Thirdly, an auto-encoder network is trained to encode an efficient representation of the waveform. Lastly, multi-resolution analysis will give frequency–time information. Next, PCA is used to reduce the dimension of the feature space by finding the principal components. For clustering four methods are tested and compared: k-means, fuzzy c-means, hierarchical cluster and a self-organizing map. The clusters can be visualized and compared with force-displacement data to identify the damage mode of each cluster. Finally, the performance of the pipeline can be evaluated using classification metrics, clustering indexes and a confusion matrix. The clustering indexes relates to the ”differentiation” aspect of the research question, while classification metrics answer the ”identification” aspect.

When this research is completed, there will be a better insight into how AE can be used to determine damage modes and their propagation in composite materials under compression and fatigue loading. Furthermore, there will be a clearer physical understanding of the damage modes and their propagation in CFRPs during compression and fatigue loading after impact. With this understanding, future research into acoustic emission used on CFRPs can answer more questions such as the usage of AE for damage evaluation in different, more complex composite structures. Also, because it is still impossible to simulate the acoustic emission coming from different composite materials, a large database of tests performed on them can be very useful for future research.

References

[1] Brown, G., "The Use of Composites in Aircraft Construction," 2014. URL https://vandaair.com/2014/04/14/the-use-of-composites-in-aircraft-construction/.

[2] Bachmann, J., Hidalgo, C., and Bricout, S., "Environmental analysis of innovative sustainable composites with potential use in aviation sector—A life cycle assessment review," *Science China Technological Sciences*, Vol. 60, No. 9, 2017, pp. 1301–1317. https://doi.org/10.1007/s11431-016-9094-y.

[3] Prichard, J. C., and Hogg, P. J., "The role of impact damage in post-impact compression testing," *Composites*, Vol. 21, No. 6, 1990, pp. 503–511. https://doi.org/10.1016/0010-4361(90)90423-T.

[4] Olsson, R., "Mass criterion for wave controlled impact response of composite plates," *Composites Part A: Applied Science and Manufacturing*, Vol. 31, No. 8, 2000, pp. 879–887. https://doi.org/10.1016/S1359-835X(00)00020-8.

[5] Olsson, R., "Low- and medium-velocity impact as a cause of failure in polymer matrix composites," *Failure Mechanisms in Polymer Matrix Composites*, 2012, pp. 53–78. https://doi.org/10.1533/9780857095329.1.53.

[6] Davies, G. A. O., and Olsson, R., "Impact on composite structures," *The Aeronautical Journal*, Vol. 108, No. 1089, 2004, pp. 541–563. https://doi.org/10.1017/S0001924000000385.

[7] Rohwer, K., "Models for intralaminar damage and failure of fiber composites - a review," *FACTA UNIVERSITATIS Series: Mechanical Engineering*, Vol. 14, No. 1, 2016, pp. 1–19.

[8] Talreja, R., "Assessment of the fundamentals of failure theories for composite materials," *Composites Science and Technology*, Vol. 105, 2014, pp. 190–201. https://doi.org/10.1016/J.COMPSCITECH.2014.10.014.

[9] Zimmermann, N., and Wang, P. H., "A review of failure modes and fracture analysis of aircraft composite materials," *Engineering Failure Analysis*, Vol. 115, 2020, p. 104692. https://doi.org/10.1016/J.ENGFAILANAL.2020.104692.

[10] Echaabi, J., Trochu, F., and Gauvin, R., "Review of failure criteria of fibrous composite materials," *Polymer Composites*, Vol. 17, No. 6, 1996, pp. 786–798. https://doi.org/10.1002/PC.10671, URL https://onlinelibrary.wiley.com/doi/full/10.1002/pc.10671https://onlinelibrary.wiley.com/doi/abs/10.1002/pc.10671https://onlinelibrary.wiley.com/doi/10.1002/pc.10671.

[11] Greenhalgh, E. S., and Hiley, M. J., "Fractography of polymer composites: current status and future issues," 2007.

[12] Davies, G., and Irving, P., "Impact, post-impact strength and post-impact fatigue behaviour of polymer composites," *Polymer Composites in the Aerospace Industry*, 2015, pp. 231–259. https://doi.org/10.1016/B978-0-85709-523-7.00009-8.

[13] Liu, D., "Impact-Induced Delamination—A View of Bending Stiffness Mismatching," *Journal of Composite Materials*, Vol. 22, No. 7, 1988, pp. 674–692. https://doi.org/10.1177/002199838802200706.

[14] Joshi, S., and Sun, C., "Impact Induced Fracture in a Laminated Composite," *Journal of Composite Materials*, Vol. 19, No. 1, 1985, pp. 51–66. https://doi.org/10.1177/002199838501900104.

[15] Wu, H.-Y. T., and Springer, G. S., "Measurements of Matrix Cracking and Delamination Caused by Impact on Composite Plates," *Journal of Composite Materials*, Vol. 22, No. 6, 1988, pp. 518–532. https://doi.org/10.1177/002199838802200602.

[16] Chang, F.-K., Choi, H. Y., and Jeng, S.-T., "Study on impact damage in laminated composites," *Mechanics of Materials*, Vol. 10, No. 1-2, 1990, pp. 83–95. https://doi.org/10.1016/0167-6636(90)90019-C.

[17] Richardson, M., and Wisheart, M., "Review of low-velocity impact properties of composite materials," *Composites Part A: Applied Science and Manufacturing*, Vol. 27, No. 12, 1996, pp. 1123–1131. https://doi.org/10.1016/1359-835X(96)00074-7.

[18] Abrate, S., "Impact on Laminated Composite Materials," 1991. https://doi.org/10.1115/1.3119500, URL https://www.researchgate.net/publication/245371355.

[19] Caprino, G., "Residual Strength Prediction of Impacted CFRP Laminates:," *http://dx.doi.org/10.1177/002199838401800601*, Vol. 18, No. 6, 2016, pp. 508–518. https://doi.org/10.1177/002199838401800601, URL https://journals.sagepub.com/doi/10.1177/002199838401800601.

[20] Bull, D. J., Spearing, S. M., and Sinclair, I., "Observations of damage development from compression-after-impact experiments using ex situ micro-focus computed tomography," *Composites Science and Technology*, Vol. 97, 2014, pp. 106–114. https://doi.org/10.1016/j.compscitech.2014.04.008.

[21] Pascoe, J.-A., "Slow-growth damage tolerance for fatigue after impact in FRP composites: Why current research won't get us there," *Theoretical and Applied Fracture Mechanics*, Vol. 116, 2021, p. 103127. https://doi.org/10.1016/j.tafmec.2021.103127, URL https://linkinghub.elsevier.com/retrieve/pii/S0167844221002287.

[22] Nettles, A. T., and Scharber, L., "The Influence of GI and GII on the compression after impact strength of carbon fiber/epoxy laminates," *Journal of Composite Materials*, Vol. 52, No. 8, 2018, pp. 991–1003. https://doi.org/10.1177/0021998317719567.

[23] Bogenfeld, R., and Gorsky, C., "An experimental study of the cyclic compression after impact behavior of cfrp composites," *Journal of Composites Science*, Vol. 5, No. 11, 2021. https://doi.org/10.3390/jcs5110296.

[24] Isa, M. D., Feih, S., and Mouritz, A. P., "Compression fatigue properties of z-pinned quasi-isotropic carbon/epoxy laminate with barely visible impact damage," *Composite Structures 93*, 2011, pp. 2269–2276. https://doi.org/10.1016/j.compstruct.2011.03.015.

[25] Ogasawara, T., Sugimoto, S., Katoh, H., and Ishikawa, T., "Fatigue behavior and lifetime distribution of impact-damaged carbon fiber/toughened epoxy composites under compressive loading," *Advanced Composite Materials 22*, 2013, pp. 65–78. https://doi.org/10.1080/09243046.2013.768324.

[26] Chen, A. S., Almond, D. P., and Harris, B., "Impact damage growth in composites under fatigue conditions monitored by acoustography," *International Journal of Fatigue 24*, 2002, pp. 257–261. https://doi.org/10.1016/S0142-1123(01)00080-9.

[27] Mitrovic, M., Hahn, H. T., Carman, G. P., and Shyprykevich, P., "Effect of loading parameters on the fatigue behavior of impact damaged composite laminates," *Composites Science and Technology 59*, 1999, pp. 2059–2078. https://doi.org/10.1016/s0266-3538(99)00061-5.

[28] Tuo, H., Wu, T., Lu, Z., and Ma, X., "Evaluation of damage evolution of impacted composite laminates under fatigue loadings by infrared thermography and ultrasonic methods," *Polymer Testing*, Vol. 93, 2021. https://doi.org/10.1016/j.polymertesting.2020.106869.

[29] Hagemaier, D., McFaul, H. J., and Moon, D., "Nondestructive Testing of Graphite Fiber Composite Structures," Tech. rep., Defense Technical Information Center, Fort Belvoir, 1970.

[30] Saeedifar, M., Najafabadi, M. A., Zarouchas, D., Toudeshky, H. H., and Jalalvand, M., "Barely visible impact damage assessment in laminated composites using acoustic emission," *Composites Part B: Engineering*, Vol. 152, 2018, pp. 180–192. https://doi.org/10.1016/j.compositesb.2018.07.016.

[31] Eitzen, D., and Wadley, H., "Acoustic Emission: Establishing the Fundamentals," *Journal of Research of the National Bureau of Standards*, Vol. 89, No. 1, 1984, p. 75. https://doi.org/10.6028/jres.089.008.

[32] Rescalvo, F. J., Valverde-Palacios, I., Suarez, E., Roldán, A., and Gallego, A., "Monitoring of carbon fiber-reinforced old timber beams via strain and multiresonant acoustic emission sensors," *Sensors (Switzerland)*, Vol. 18, No. 4, 2018. https://doi.org/10.3390/s18041224.

[33] Khayal, S., and Elmardi, O. M., "Literature review on imperfection of composite laminated plates," *Journal of Microscopy and Ultrastructure*, Vol. 5, No. 3, 2017, pp. 119–122. https://doi.org/10.1016/J.JMAU.2017.01.001.

[34] Kharrat, M., Placet, V., Ramasso, E., and Boubakar, M. L., "Influence of damage accumulation under fatigue loading on the AE-based health assessment of composite materials: Wave distortion and AE-features evolution as a function of damage level," *Composites Part A: Applied Science and Manufacturing*, Vol. 109, 2018, pp. 615–627. https://doi.org/10.1016/J.COMPOSITESA.2016.03.020.

[35] Saeedifar, M., and Zarouchas, D., "Damage characterization of laminated composites using acoustic emission: A review," *Composites Part B: Engineering*, Vol. 195, 2020, p. 108039. https://doi.org/10.1016/j.compositesb.2020.108039, URL https://linkinghub.elsevier.com/retrieve/pii/S1359836819365096.

[36] Grosse, C. U., and Ohtsu, M., *Acoustic emission testing: Basics for Research-Applications in Civil Engineering*, Springer Berlin Heidelberg, 2008. https://doi.org/10.1007/978-3-540-69972-9.

[37] Shateri, M., Ghaib, M., Svecova, D., and Thomson, D., "On acoustic emission for damage detection and failure prediction in fiber reinforced polymer rods using pattern recognition analysis," *Smart Materials and Structures*, Vol. 26, No. 6, 2017. https://doi.org/10.1088/1361-665X/aa6e43.

[38] Sun, Q., Zhou, G., Guo, H., Meng, Z., Chen, Z., Liu, H., Kang, H., and Su, X., "Failure mechanisms of cross-ply carbon fiber reinforced polymer laminates under longitudinal compression with experimental and computational analyses," *Composites Part B: Engineering*, Vol. 167, 2019, pp. 147–160. https://doi.org/10.1016/j.compositesb.2018.12.041.

[39] Prosser, W. H., Jackson, K. E., Kellas, S., Smith, B. T., Mckeon, J., and Friedman, A., "Advanced, Waveform Based Acoustic Emission Detection of Matrix Cracking in Composites," Tech. Rep. 9, 1995.

[40] Pashmforoush, F., Khamedi, R., Fotouhi, M., Hajikhani, M., and Ahmadi, M., "Damage Classification of Sandwich Composites Using Acoustic Emission Technique and k-means Genetic Algorithm," *Journal of Nondestructive Evaluation*, Vol. 33, No. 4, 2014, pp. 481–492. https://doi.org/10.1007/s10921-014-0243-y.

[41] Bakhtiary Davijani, A. A., Hajikhani, M., and Ahmadi, M., "Acoustic Emission based on sentry function to monitor the initiation of delamination in composite materials," *Materials and Design*, Vol. 32, No. 5, 2011, pp. 3059–3065. https://doi.org/10.1016/j.matdes.2011.01.010.

[42] Gutkin, R., Green, C. J., Vangrattanachai, S., Pinho, S. T., Robinson, P., and Curtis, P. T., "On acoustic emission for failure investigation in CFRP: Pattern recognition and peak frequency analyses," *Mechanical Systems and Signal Processing*, Vol. 25, No. 4, 2011, pp. 1393–1407. https://doi.org/10.1016/J.YMSSP.2010.11.014.

[43] Tsamtsakis, D., Wevers, M., and de Meester, P., "Tsamtsakis - Acoustic Emissions from CFRP LAminates during Fatigue Loading," *Journal of Reinforced Plastics and Composites*, Vol. 17, No. 13, 1998, pp. 1185–1201.

[44] Bourchak, M., Farrow, I. R., Bond, I. P., Rowland, C. W., and Menan, F., "Acoustic emission energy as a fatigue damage parameter for CFRP composites," *International Journal of Fatigue*, Vol. 29, No. 3, 2007, pp. 457–470. https://doi.org/10.1016/J.IJFATIGUE.2006.05.009.

[45] Woo, S. C., and Kim, T. W., "High strain-rate failure in carbon/Kevlar hybrid woven composites via a novel SHPB-AE coupled test," *Composites Part B: Engineering*, Vol. 97, 2016, pp. 317–328. https://doi.org/10.1016/J.COMPOSITESB.2016.04.084.

[46] de Groot, P. J., Wijnen, P. A., and Janssen, R. B., "Real-time frequency determination of acoustic emission for different fracture mechanisms in carbon/epoxy composites," *Composites Science and Technology*, Vol. 55, No. 4, 1995, pp. 405–415.

[47] Saeedifar, M., Najafabadi, M. A., Zarouchas, D., Toudeshky, H. H., and Jalalvand, M., "Clustering of interlaminar and intralaminar damages in laminated composites under indentation loading using Acoustic Emission," *Composites Part B: Engineering*, Vol. 144, 2018, pp. 206–219. https://doi.org/10.1016/j.compositesb.2018.02.028, URL https://linkinghub.elsevier.com/retrieve/pii/S1359836817343718.

[48] Murtagh, F., and Heck, A., *Multivariate Data Analysis*, Astrophysics and Space Science Library, Vol. 131, Springer Netherlands, Dordrecht, 1987. https://doi.org/10.1007/978-94-009-3789-5, URL http://link.springer.com/10.1007/978-94-009-3789-5.

[49] Brunton, S. L., and Kutz, J. N., *Data-Driven Science and Engineering*, Cambridge University Press, 2019. https://doi.org/10.1017/9781108380690.

[50] Saeedifar, M., Saleh, M. N., El-Dessouky, H. M., Teixeira De Freitas, S., and Zarouchas, D., "Damage assessment of NCF, 2D and 3D woven composites under compression after multiple-impact using acoustic emission," *Composites Part A: Applied Science and Manufacturing*, Vol. 132, 2020, p. 105833. https://doi.org/10.1016/j.compositesa.2020.105833, URL https://linkinghub.elsevier.com/retrieve/pii/S1359835X20300713.

[51] Donoho, D. L., and Johnstone, I. M., "Ideal Spatial Adaptation by Wavelet Shrinkage," *Biometrika*, Vol. 81, No. 3, 1994, p. 455. https://doi.org/10.2307/2337118.

[52] Gilles, J., "Empirical Wavelet Transform," *IEEE Transactions on Signal Processing*, Vol. 61, No. 16, 2013, pp. 3999–4010. https://doi.org/10.1109/TSP.2013.2265222.

[53] Bianco, M. J., Gerstoft, P., Traer, J., Ozanich, E., Roch, M. A., Gannot, S., and Deledalle, C.-A., "Machine learning in acoustics: Theory and applications," *The Journal of the Acoustical Society of America*, Vol. 146, No. 5, 2019, pp. 3590–3628. https://doi.org/10.1121/1.5133944, URL http://asa.scitation.org/doi/10.1121/1.5133944.

[54] Van Der Maaten, L., Postma, E., and Van Den Herik, J., "Dimensionality Reduction: A Comparative Review," Tech. rep., Tilburg centre for Creative Computing, Tilburg, 2009. URL http://www.uvt.nl/ticc.

[55] Candès, E. J., Wright, J., Li, X., and Ma, Y., "Robust principal component analysis," *Journal of the ACM*, Vol. 58, No. 3, 2011. https://doi.org/10.1145/1970392.1970395, URL http://doi.acm.org/10.1145/1970392.1970395.

[56] Bezdek, J. C., Ehrlich, R., and Full, W., "FCM: The fuzzy c-means clustering algorithm," *Computers & geosciences*, Vol. 10, No. 2-3, 1984, pp. 191–203.

[57] Liu, C., Nagler, O., Tremmel, F., Unterreitmeier, M., Frick, J. J., Patil, R. P., Gu, X. W., and Senesky, D. G., "Cluster-based acoustic emission signal processing and loading rate effects study of nanoindentation on thin film stack structures," *Mechanical Systems and Signal Processing*, Vol. 165, 2022, p. 108301. https://doi.org/10.1016/j.ymssp.2021.108301.

[58] "Standard Test Method for Measuring the Damage Resistance of a Fiber-Reinforced Polymer Matrix Composite to a Drop-Weight Impact Event 1," *ASTM International*, 2021. https://doi.org/10.1520/D7136{_}D7136M-20, URL www.astm.org,.

[59] "Standard Test Method for Compressive Residual Strength Properties of Damaged Polymer Matrix Composite Plates," *ASTM International*, 2021. https://doi.org/10.1520/D7137{_}D7137M-17, URL www.astm.org,.

[60] Vallen Systeme GmbH, "Acoustic Emission Sensors and Preamplifiers Description," Tech. rep., 2021. URL http://www.vallen.de.

[61] "Template Project Proposal and Plan," Tech. rep., 2013.

Appendices

A. Gantt Chart

A Gantt chart was created in Section 7 to visualize the logistics of the project. Below, the Gantt chart is shown again with more detailed dates.

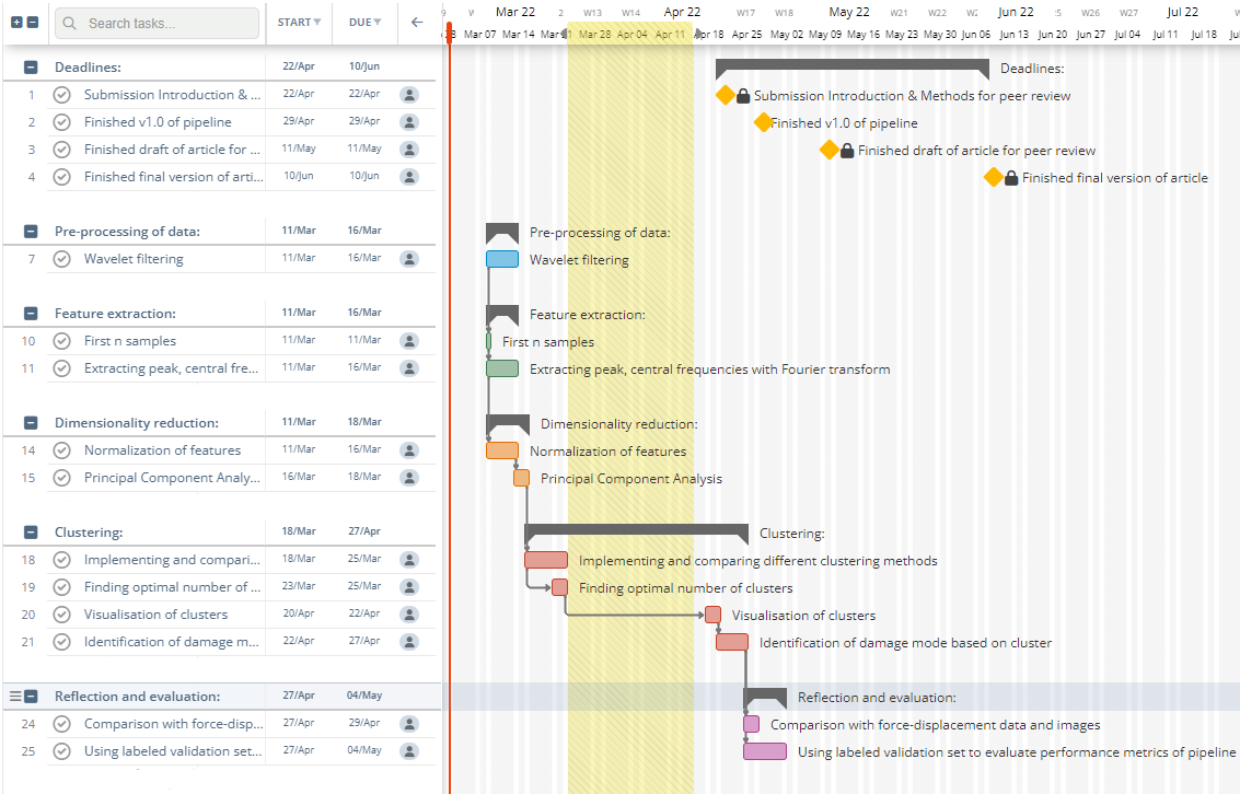

Figure 13: *Detailed Gantt chart based on the work packages* [1]